

## The Loss-cone Driven Electron-cyclotron Maser

R. G. Hewitt,<sup>A</sup> D. B. Melrose<sup>A</sup> and K. G. Rönmark<sup>B</sup>

<sup>A</sup> School of Physics, University of Sydney, Sydney, N.S.W. 2006.

<sup>B</sup> Kiruna Geophysical Institute, University of Umeå, S-901 87 Umeå, Sweden.

### Abstract

Electron-cyclotron instabilities may be classified in two ways depending on whether the relativistic correction to the gyrofrequency is important (class S) or not (class N), and whether the instability mechanism is of a maser type (class M) or due to bunching (class B). Renewed interest in class SM has followed the Wu and Lee application of it to the interpretation of terrestrial kilometric radiation. The maser is assumed to be driven by a one-sided loss-cone distribution of electrons. This mechanism seems particularly favourable for the interpretation of certain planetary, solar and stellar radio emissions.

The loss-cone driven SM instability is explored in detail here through numerical calculations of the growth rate and the development of a semi-quantitative theory for the maser mechanism. The numerical calculations are for a hot Maxwellian distribution with a hole in pitch angle  $\alpha$ ; the distribution falls off with pitch angle inside the loss cone  $\alpha > \alpha_0$  ( $> \frac{1}{2}\pi$ ) as a power of a sine function of  $\alpha - \alpha_0$ . It is assumed that the dispersive properties of the waves are determined by a cold plasma (with frequency  $\omega_p$ ) and only emission in the x mode and the o mode above their respective cutoff frequencies is considered. The semi-quantitative theory involves the parameters  $\alpha_0$  and the characteristic range of  $|\alpha - \alpha_0|$  over which the distribution falls off inside the loss cone  $\Delta\alpha$ , the energy  $\frac{1}{2}mv_m^2$  and the number density  $n_H$  of the energetic electrons, and the ratio  $\omega_p/\Omega_e$ , with  $\Omega_e$  the electron-cyclotron frequency.

The maser emission is possible at all harmonics  $s = 1, 2, \dots$  ( $\omega \approx s\Omega_e$ ) and occurs just above the relevant harmonic. The maximum growth rate falls off with increasing  $s$  roughly as  $(v_m/c)^{2s} \sin^{2s}\alpha_0$  and is smaller for the o mode than the x mode by a factor  $\approx (v_m/c)^2$ . The effective growth is confined to a narrow range of angles  $\Delta\theta \lesssim (v_m/c)\sin\alpha_0$  about the surface of a cone with half-angle  $\theta_m \approx \arccos(v_m/c)$ . The frequency range at fixed  $\theta$  is very narrow, with  $\Delta\omega/s\Omega_e \approx (v_m/c)^2 \Delta\alpha \sin\alpha_0$ . Emission of the x mode at  $s = 1$  is quite strongly suppressed (from what it would be for negligible  $\omega_p$ ) for  $\omega_p/\Omega_e \gtrsim \frac{1}{2}v_m/c$ , and is noticeably suppressed even for much smaller values of  $\omega_p/\Omega_e$ .

An application of the mechanism to the interpretation of the Jovian decametric radio emissions is outlined.

### 1. Introduction

In the astrophysical literature over the past few years there has been renewed interest in electron-cyclotron maser emission in connection with the interpretation of certain planetary, solar and stellar radio emissions. The renewed interest was initiated by Wu and Lee (1979) who pointed out that when the Lorentz factor  $\gamma = (1 - v^2/c^2)^{-\frac{1}{2}}$  is approximated by  $\gamma = 1 + v^2/2c^2$ , the resonance condition  $\omega - s\Omega_e/\gamma - k_{\parallel}v_{\parallel} = 0$  has qualitatively different solutions from the strictly non-relativistic case  $\gamma = 1$ . In particular, the equation becomes quadratic in  $v_{\parallel}$  and hence has two solutions rather than the single solution for  $\gamma = 1$ . It is now recognized that the exact resonance condition corresponds to an ellipse in  $v_{\perp}-v_{\parallel}$  space (Hewitt

*et al.* 1981). The ellipse becomes highly eccentric for  $k_{\parallel}^2 c^2 \gg \omega^2$ , when it may be approximated by the straight line  $v_{\parallel} = (\omega - s\Omega_e)/k_{\parallel}$ , and it becomes nearly circular for  $\omega^2 \gg k_{\parallel}^2 c^2$ . Let us refer to these limiting cases as the nonrelativistic (N) and semirelativistic (S) limits respectively. Electron-cyclotron maser emission in the S limit has some peculiar features which were not anticipated before the Wu and Lee discussion. These features include (a) the maser emission is above the cyclotron harmonic frequency, as opposed to below it in the N limit (Melrose 1973), (b) the emission may be confined to a narrow range of angles  $\theta$  and/or to a narrow frequency range, and (c) it can be driven by a distribution with a loss-cone anisotropy under surprisingly mild conditions. The fact that a loss-cone anisotropy can be set up readily whenever electrons precipitate from a magnetosphere or a magnetic trap suggests that this type of electron-cyclotron maser emission might be common in situations of astrophysical interest.

In this paper we explore the loss-cone driven electron-cyclotron instability in detail for a specific analytic distribution of electrons. In particular we choose a Maxwellian distribution with a hole corresponding to a one-sided loss cone; the distribution varies as a power of a sine function of  $\alpha - \alpha_0$ , where the pitch angle  $\alpha = \alpha_0$  denotes the edge of the loss cone. Our main purpose is to elucidate and quantify the main features of this instability. To this end we also develop a semi-quantitative theory which complements our detailed calculations. Before proceeding with this discussion let us place the present interest in S-type maser instabilities and their suggested applications in context.

Cyclotron instabilities may be classified in two complementary ways. One is the classification N and S introduced above. The other is into maser (M) mechanisms, which involve negative absorption, and bunching (B) instabilities, which occur for monoenergetic particles. This second classification corresponds to Briggs' (1964) 'resistive-medium' and 'reactive-medium' instabilities respectively, and to the distinction between 'kinetic' and 'hydrodynamic' instabilities respectively in the Russian literature. There are thus four classes of cyclotron instability: SM, NM, SB and NB. We are concerned with SM instabilities.

Class SM instabilities were amongst the first discussed in the literature by Twiss (1958), Schneider (1959) and Bekefi *et al.* (1961) (cf. also Bekefi 1966, p. 302). In these earlier discussions the resonance condition was artificially reduced to the form  $\omega - s\Omega_e/\gamma = 0$ , either by assuming  $v_{\parallel} = 0$ , as done by Twiss (1958) and Schneider (1959), or by assuming perpendicular propagation  $k_{\parallel} = 0$ , as done by the other authors cited. The renewed interest in SM instabilities arose when the implications of relaxing this assumption were recognized by Wu and Lee (1979). The existence of the other classes of instability were also recognized around 1960; the class NM by Sagdeev and Shafranov (1960) (cf. also Stix 1962, p. 207), and classes NB and SB by Gaponov (1959*a*, 1959*b* respectively). The relation between NM and NB instabilities was discussed by Melrose (1973), that between NB and SB by Sprangle and Drobot (1977) and Chu and Hirshfield (1978), and that between SM and SB by Winglee (1982). Broadly speaking, NM instabilities apply to the growth of waves in magnetized plasmas due to anisotropic distributions of particles, and SB instabilities to laboratory gyrotrons.

The suggested astrophysical applications of SM instabilities are to the Jovian decametric radiation (DAM), to the terrestrial kilometric radiation (TKR) and analogous radiation from Saturn (SKR), to solar microwave spike bursts and to bright

radio emission from some flare stars. Earlier cyclotron theories for DAM included examples of NB and SB instabilities (see e.g. Ellis and McCulloch 1963; Ellis 1965; Fung 1966; Goldreich and Lynden-Bell 1969) and of NM instabilities (see e.g. Chang 1963; Goldstein and Eviatar 1972, 1979; Melrose 1973, 1976). Parenthetically we remark that although Goldstein and Eviatar (1972, 1979) considered a loss-cone driven NM instability for directly escaping radiation, this work contained an error (Goldstein and Goertz 1982) and the existence of loss-cone driven NM instabilities for  $k \leq \omega/c$  is unproven. There was also an earlier suggestion of an SM instability for DAM by Hirshfield and Bekefi (1963), but their assumptions of perpendicular propagation, isotropic electrons and no cold plasma were unrealistic. One of the particularly favourable features of the loss-cone driven SM instability for the interpretation of DAM is the predicted emission on the surface of a hollow cone (Hewitt *et al.* 1981). There is strong observational evidence for such an unusual emission pattern both from Earth-based observations (Dulk 1967) and from the nested-arc pattern observed from VOYAGERS 1 and 2 (see e.g. Goldstein and Thieman 1981). TKR has some properties similar to those of DAM and is known to correlate closely with 'inverted-V' precipitating electrons. Recently, observational data on such electrons have been used to determine the distribution function  $f(p_{\perp}, p_{\parallel})$ , which has then been used to calculate the growth rate for the SB instability (Melrose *et al.* 1982; Omidi and Gurnett 1982; Wu *et al.* 1982). It has been shown that an observed one-sided loss-cone feature due to reflected electrons is capable of driving the instability as proposed by Wu and Lee (1979) (cf. also Lee *et al.* 1980; Lee and Wu 1980; Wu *et al.* 1982). An important detail is that the instability requires a plasma frequency  $\omega_p$  much less than the electron-cyclotron frequency  $\Omega_e$ , and this inequality is satisfied in the source region for TKR (Benson and Calvert 1979). The suggested application of SM instabilities to solar spike bursts was proposed by Holman *et al.* (1980) and has been discussed in more detail by Melrose and Dulk (1982*a*, 1982*b*).

In Section 2 we review the geometric interpretation of the resonance condition in terms of a resonant ellipse and point out why a loss-cone distribution is particularly favourable for wave growth. In Section 3 we report the results of our numerical calculations of the growth rate. We consider the growth rate as a function of (a) angle  $\theta$ , (b) frequency and (c) steepness of the distribution within the loss cone. We discuss both the x mode and the o mode at  $s = 1$ , and also the x mode at  $s = 2$ . In Section 4 we consider the implications of the existence of 'boundary curves' in  $\omega$ - $\theta$  space defined by the vanishing of the resonant ellipse. In Section 5 we discuss the effect of a variation in  $\omega_p/\Omega_e$  and provide a qualitative interpretation of a suppression which occurs for the x mode at  $s = 1$  when  $\omega_p/\Omega_e$  exceeds a quite modest value. In Section 6 we develop a semi-qualitative theory which is consistent with our numerical results and which offers a physical interpretation of several important features of the maser emission. In Section 7 we discuss one application, specifically to DAM, to illustrate the use of our results.

## 2. Resonant Ellipse and Growth Rate

In this section we present the geometric interpretation of the resonance condition in terms of a resonant ellipse, following Hewitt *et al.* (1981). We then summarize the relevant wave properties, write down a formula for the growth rate and comment on several of its features.

(a) *Resonant Ellipse*

The resonance condition

$$\omega - s\Omega_e/\gamma - k_{\parallel} v_{\parallel} = 0, \quad (1)$$

with  $\gamma = (1 - v^2/c^2)^{-\frac{1}{2}}$  corresponds to an ellipse in  $v_{\perp}$ - $v_{\parallel}$  space. (Actually the physical curve is a semi-ellipse restricted to  $v_{\perp} \geq 0$ , but for simplicity we refer to it consistently as an ellipse.) The ellipse is centred at

$$v_{\parallel}/c = \omega k_{\parallel} c / (k_{\parallel}^2 c^2 + s^2 \Omega_e^2), \quad v_{\perp}/c = 0, \quad (2a, b)$$

and has an eccentricity

$$e = \{k_{\parallel}^2 c^2 / (k_{\parallel}^2 c^2 + s^2 \Omega_e^2)\}^{\frac{1}{2}}, \quad (3)$$

and semi-major axis, parallel to the  $v_{\perp}$  axis,

$$V/c = \{(k_{\parallel}^2 c^2 + s^2 \Omega_e^2 - \omega^2) / (k_{\parallel}^2 c^2 + s^2 \Omega_e^2)\}^{\frac{1}{2}}. \quad (4)$$

The nonrelativistic (N) and semirelativistic (S) approximations are relevant only in the region  $v^2/c^2 \ll 1$  and correspond to  $e \approx 1$  and  $e \approx 0$  respectively. In the S limit the ellipse may be approximated by a circle centred at

$$v_{\parallel}/c = k_{\parallel} c / \omega, \quad v_{\perp}/c = 0, \quad (5a, b)$$

with radius

$$\frac{V}{c} = \left( \frac{k_{\parallel}^2 c^2}{\omega^2} - \frac{2(\omega - s\Omega_e)}{s\Omega_e} \right)^{\frac{1}{2}}. \quad (6)$$

Note that the position and shape of the resonant ellipse is uniquely determined by specifying  $s\Omega_e$ ,  $\omega$  and  $k_{\parallel}$ . For waves in any given mode, the dispersion relation determines  $k_{\parallel}$  in terms of  $\omega$  and  $\theta$ . Hence, once  $\omega$  and  $\theta$  are specified, the resonant ellipse at each harmonic  $s$  is determined. In practice there is only a localized region of  $v_{\perp}$ - $v_{\parallel}$  space in which the conditions for wave growth are favourable, and the waves which grow are those whose resonant ellipses lie entirely or predominantly within this region.

(b) *Wave Properties*

We are concerned with waves which can escape from the plasma. These are the magnetoionic waves in the o mode at  $\omega > \omega_p$  and in the x mode at  $\omega > \omega_x$ , where

$$\omega_x = \frac{1}{2}\Omega_e + \frac{1}{2}(\Omega_e^2 + 4\omega_p^2)^{\frac{1}{2}}. \quad (7)$$

These waves have a refractive index less than unity, and hence  $|k_{\parallel} c/\omega| < 1$ .

The wave properties are given by (Melrose 1980*b*, p. 258):

$$n_{\sigma}^2 = 1 - \frac{XT_{\sigma}}{T_{\sigma} - Y \cos \theta}, \quad K_{\sigma} = \frac{XY \sin \theta}{1 - X} \frac{T_{\sigma}}{T_{\sigma} - Y \cos \theta}, \quad (8a, b)$$

$$T_{\sigma} = -\sigma(x^2 + 1)^{\frac{1}{2}} - x, \quad x = Y \sin^2 \theta / 2(1 - X) \cos \theta, \quad (8c, d)$$

$$X = \omega_p^2 / \omega^2, \quad Y = \Omega_e / \omega, \quad (8e, f)$$

where  $\sigma$  labels the mode, with  $\sigma = 1$  for the o mode and  $\sigma = -1$  for the x mode,  $n_{\sigma}$  is the refractive index, and  $K_{\sigma}$  and  $T_{\sigma}$  describe the polarization of the waves.

(c) *Growth Rate*

A general formula for the growth rate at the  $s$ th harmonic for waves in the magneto-ionic modes is (Melrose 1980*b*, p. 275)

$$\Gamma_s^{(\sigma)}(\mathbf{k}) = \int d\mathbf{p} A_s^{(\sigma)}(\mathbf{p}, \mathbf{k}) \delta(\omega - s\Omega_e/\gamma - k_{\parallel} v_{\parallel}) \left( \frac{s\Omega_e}{\gamma v_{\perp}} \frac{\partial}{\partial p_{\perp}} + k_{\parallel} \frac{\partial}{\partial p_{\parallel}} \right) f(p_{\perp}, p_{\parallel}), \quad (9)$$

where

$$A_s^{(\sigma)}(\mathbf{p}, \mathbf{k}) = \frac{4\pi^2 e^2 v_{\perp}^2}{\omega n_{\sigma} \{ \partial(\omega n_{\sigma}) / \partial \omega \} (1 + T_{\sigma}^2)} \left| \frac{K_{\sigma} \sin \theta + (\cos \theta - n_{\sigma} v_{\parallel}/c) T_{\sigma}}{n_{\sigma} (v_{\perp}/c) \sin \theta} J_s + J'_s \right|^2, \quad (10)$$

with  $J_s$  and  $J'_s$  respectively a Bessel function and its derivative with argument  $(\omega/\Omega_e) n_{\sigma} (v_{\perp}/c) \sin \theta$ .

Hewitt *et al.* (1981) showed that the triple integral in (9) could be reduced to a single integral around the circumference of the resonant ellipse. At each point on the circumference the sign of the integrand is determined by the sign of the sum of the two terms involving derivatives in (9). Growth requires that the net positive contribution exceeds any net negative contribution around the ellipse.

In the S limit one has  $|k_{\parallel}| \ll \omega/c$  and with  $\omega \approx s\Omega_e$  the coefficient of the  $p_{\parallel}$  derivative in (9) is much smaller than the coefficient of the  $p_{\perp}$  derivative. An SM instability therefore requires  $\partial f / \partial p_{\perp} > 0$ . A loss-cone distribution has a deficiency or absence of particles with small  $\sin \alpha$ , and hence is an increasing function of  $\sin \alpha$  for small  $\sin \alpha$ . This corresponds to being an increasing function of  $p_{\perp}$  inside the loss cone. Waves corresponding to resonant ellipses which lie entirely within the loss cone then have a positive growth rate. The maximum growth occurs for that ellipse with the largest (weighted) integrated value of  $\partial f / \partial p_{\perp}$ . By implication any loss-cone distribution is subjected to an SM instability. The requirement that the frequency be greater than the cutoff frequency ( $\omega = \omega_p$  for the o mode and  $\omega = \omega_x$  for the x mode) implies that electron-cyclotron maser emission is stronger for small values of  $\omega_p/\Omega_e$  when  $s = 1$ .

### 3. Detailed Results

In this section we summarize the results of numerical calculations for the growth rate (9) for the x mode at  $s = 1, 2$  and the o mode at  $s = 1$ . Throughout, the rate  $\omega_p/\Omega_e$  is fixed at 0.1 and the loss-cone angle at  $\alpha_0 = 150^\circ$  (these assumptions are relaxed in Sections 5 and 6 respectively). Relativistic effects are ignored except in the resonance condition.

The distribution function chosen is Maxwellian with a hole:

$$f(p_{\perp}, p_{\parallel}) = n_H g_N(\alpha) (1/2\pi mKT)^{3/2} \exp(-mv^2/2KT), \quad (11)$$

with

$$g_N(\alpha) = a_N, \quad \alpha \leq \alpha_0, \quad (12a)$$

$$= a_N [\sin \{ \frac{1}{2} \pi (\pi - \alpha) / (\pi - \alpha_0) \}]^N, \quad \alpha > \alpha_0. \quad (12b)$$

In (11),  $n_H$  is the number density of the hot electrons and is assumed much less than the number density  $n_C$  of the cold electrons; thus we have  $\omega_p^2 = n_C e^2 / \epsilon_0 m$ . Specifically it is assumed that the cold electrons determine the dispersive properties of the waves

and the hot electrons determine their absorption or growth rate. The parameter  $N$  in (12) determines the steepness of the edge of the loss cone, with large  $N$  corresponding to  $f$  dropping rapidly to zero just inside the loss cone. The normalization coefficient  $a_N$  is close to unity for all cases of interest, as shown by the following tabulation for all values of  $N$  used in the detailed calculations:

$N$	1	2	3	4	5	6
$(a_N - 1) \times 10^2$	1.30	2.06	2.57	2.94	3.24	3.47

We approximate  $a_N$  by unity in our detailed results, which leads to errors of only a few per cent.

The growth rate is proportional to  $n_H$ . Our results are for the specific numerical values  $n_H = 10^{13} \text{ m}^{-3}$ ,  $n_C = 10^{15} \text{ m}^{-3}$  and  $\Omega_e/2\pi = 3 \text{ GHz}$ . However, the growth rate may be plotted as a fraction of  $\Omega_e$  and then the functional dependence involves only the ratios  $n_H/n_C$ ,  $\omega_p/\Omega_e$  and  $\omega/\Omega_e$ . The other parameters are chosen to be  $T = 10^8 \text{ K}$  and  $N$  in the range 1 to 6.

#### (a) x Mode at $s = 1$

The variation with  $\omega$  and  $\theta$  of the growth rate for the x mode at the fundamental  $s = 1$  is illustrated in Figs 1–3. In Fig. 1 a selection of  $\theta$  values is chosen and  $\Gamma$  is plotted as a function of  $\omega$ . To illustrate the variation with  $\theta$  the maxima of the curves in Fig. 1 are plotted against  $\theta$  in Fig. 2. In Fig. 3 a specific angle is chosen and the dependence of the steepness of the distribution function inside the loss cone is illustrated by plotting  $\Gamma$  as a function of  $\omega$  for  $N = 1, 3$  and 6. The resonant ellipses at which the maximum growth rates occur are shown in Fig. 4.

Note that there is a double peak in one of the curves for the smallest angle  $\theta = 105^\circ$  in Fig. 1. This may be attributed to there being two regions of growth at this angle, corresponding to two values of  $k_{\parallel}^2 c^2/\omega^2$ . The main peak is for the larger value of this quantity. Similar narrow peaks occur near the cutoff frequency for other angles of propagation, but cannot be shown in Fig. 1 because all the narrow peaks overlap. In the following discussion we concentrate almost exclusively on the peaks at the greater frequency.

#### (b) o Mode at $s = 1$

For the o mode at  $s = 1$  the growth rate has very similar properties to the x mode at  $s = 1$ . This may be seen by inspection of Figs 5–7, which are the counterparts of Figs 1–3 for the o mode rather than the x mode. The most notable change is that the growth rate for the o mode is smaller than that for the x mode by a factor of about ten. One expects this to be the case because the handedness of a spiralling electron is the same as the handedness of an x mode wave (at  $\omega > \omega_x$ ) and opposite to that of an o mode wave (at  $\omega > \omega_p$ ). A semi-quantitative discussion of this point is given in Section 6e below.

There is no double structure in any of the peaks for the o mode, or for the x mode at  $s \geq 2$  (see Fig. 8), because we have  $k^2 c^2/\omega^2 \approx 1$  throughout the regime of interest. The resonant ellipses for the o mode and for the x mode at  $s \geq 2$  are similar to those shown in Fig. 4. The maximum growth occurs for smaller ellipses closer to the origin than for the x mode at  $s = 1$ ; this is due to the suppression effect discussed in Section 5.

(c) *x Mode at  $s = 2$*

The growth rate for the *x* mode at  $s = 2$  is shown in Figs 8–10, which are analogous to Figs 1–3. The most notable change from  $s = 1$  to  $s = 2$  is the drop in the magnitude of the growth rate by a factor of  $\approx 10^2$ . The explanation for this is straightforward. It is well known that for nonrelativistic particles the strength of the gyro-magnetic interaction varies with  $s$  as  $\{n_\sigma(v_\perp/c) \sin \theta\}^{2s}$ . Inspection of Fig. 4 shows that one has  $v_\perp/c \approx 0.1$  for the relevant resonant particles, and with  $n_x \approx 1$  and  $\sin \theta \approx 1$  one would predict a drop by a factor of  $\approx 10^{-2}$  with an increase in  $s$  of unity. Otherwise the second harmonic (as a function of  $\omega/2\Omega_e$ ) is similar to the fundamental (as a function of  $\omega/\Omega_e$ ). An exception is a suppression effect for the fundamental (see Section 5).

**4. Boundary Curves**

As a first step in interpreting the foregoing results qualitatively and semi-quantitatively, we consider the ‘boundary curves’ defined by  $V = 0$ , i.e. by the vanishing of the semi-major axis of the resonant ellipse. The resonant ellipses in Fig. 4 have  $V \ll c$ , and one might anticipate that the growth is restricted to regions near  $V = 0$ . This is the case.

(a) *Boundary Curves for  $\omega_p/\Omega_e = 0$*

The boundary curve  $V = 0$  corresponds to (cf. equation 4)

$$k^2 c^2 \cos^2 \theta + s^2 \Omega_e^2 - \omega^2 = 0. \tag{13}$$

Firstly, we consider the case  $k = \omega/c$ , i.e. for  $\omega_p/\Omega_e$  negligibly small. Then in  $\omega$ - $\theta$  space, the solution of (13) defines two curves  $\theta = \theta'$  and  $\theta = \pi - \theta'$ , with

$$\theta' = \arccos\{(\omega^2 - s^2 \Omega_e^2)^{1/2} / \omega\}. \tag{14}$$

In the region  $\theta' < \theta < \pi - \theta'$  no resonance is possible. We are interested in upgoing waves and hence we concentrate on the branch at  $\theta > \frac{1}{2}\pi$ . Provided  $\omega_p/\Omega_e$  is less than unity, and not too close to unity, the boundary curves for the *o* mode at all  $s \geq 1$  and for the *x* mode at  $s \geq 2$  differ little from the vacuum case.

(b) *Boundary Curves for Magnetoionic Waves*

When we include the effect of a magnetoionic medium,  $k$ ,  $\omega$  and  $\theta$  are related by the dispersion equation (see e.g. Stix 1962, p. 11; Melrose 1980a, p. 55)

$$(P \cos^2 \theta + S \sin^2 \theta)(k^2 c^2 / \omega^2)^2 - \{(S^2 - D^2) \sin^2 \theta + PS(1 + \cos^2 \theta)\} k^2 c^2 / \omega^2 + P(S^2 - D^2) = 0, \tag{15}$$

with

$$P = 1 - (\omega_p/\Omega_e)^2 Y^2, \tag{16a}$$

$$S = 1 - (\omega_p/\Omega_e)^2 Y^2 / (1 - Y^2), \tag{16b}$$

$$D = -(\omega_p/\Omega_e)^2 Y^3 / (1 - Y^2), \tag{16c}$$

with  $Y$  defined by (8f). On eliminating  $k^2$  between (13) and (15) one obtains an equation for the boundary curves in  $\omega$ - $\theta$  space. These boundary curves are plotted in Fig. 11 for  $\omega_p/\Omega_e = 0.1$ .

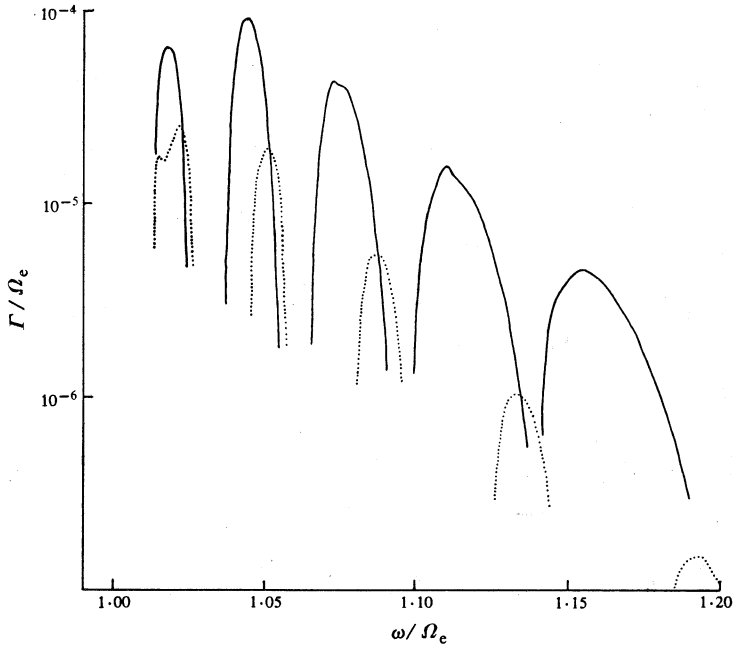


**Fig. 1.** Relative growth rate  $\Gamma/\Omega_e$  for the x mode at  $s = 1$  as a function of  $\omega/\Omega_e$  for  $\theta = 105^\circ, 110^\circ, 115^\circ, 120^\circ$  and  $125^\circ$  (from left to right). The dotted curves are for  $N = 1$  in equations (12) and the solid curves for  $N = 6$ .

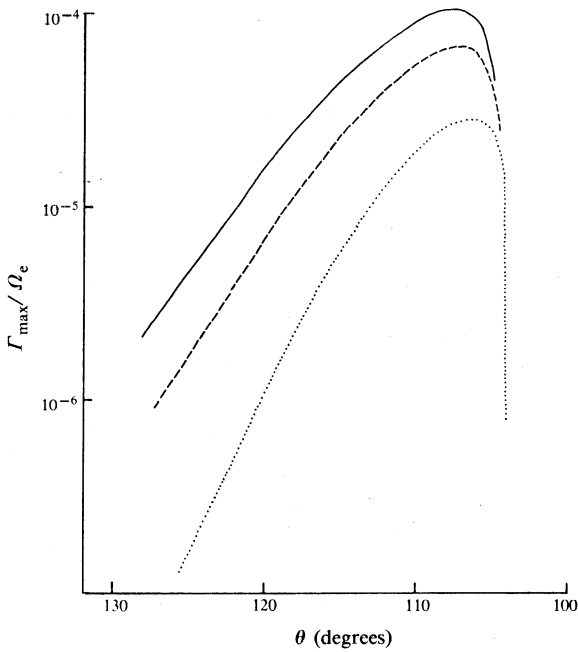


**Fig. 2.** Maxima of the curves in Fig. 1 as a function of  $\theta$  for  $N = 1$  (dotted curve),  $N = 3$  (dashed curve) and  $N = 6$  (solid curve). The sharp cutoff at  $\theta \approx 104^\circ$  is due to the suppression effect discussed in Section 5.

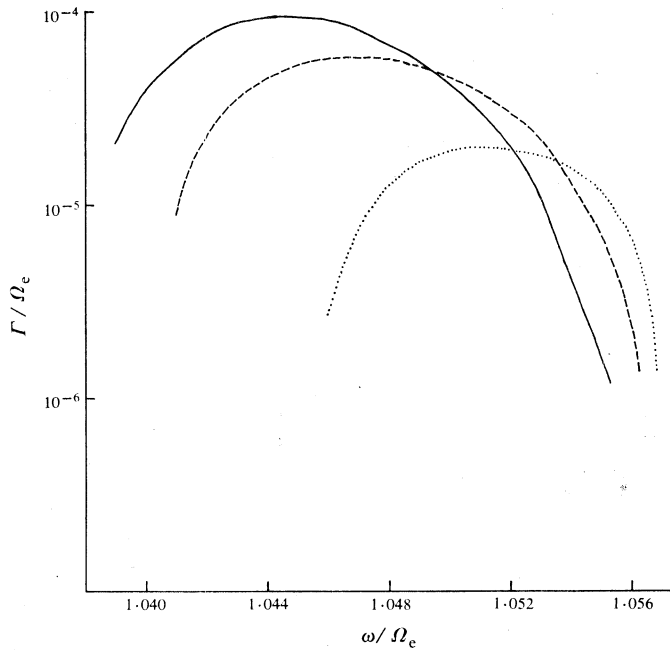


**Fig. 3.** Relative growth rate for the x mode at  $s = 1$  as a function of  $\omega/\Omega_e$  for  $\theta = 110^\circ$  for  $N = 1$  (dotted curve),  $N = 3$  (dashed curve) and  $N = 6$  (solid curve). The frequency at which the maximum occurs over the range  $N = 2$  to  $6$  is  $\omega_{\max}/\Omega_e \approx 1.050 - 0.001 N$ ; the case  $N = 1$  is anomalous. The frequency separation  $\Delta\omega_{1/2}$  between the half-maximum growth points is roughly independent of  $N$  at  $\Delta\omega_{1/2}/\Omega_e \approx 0.009$ .

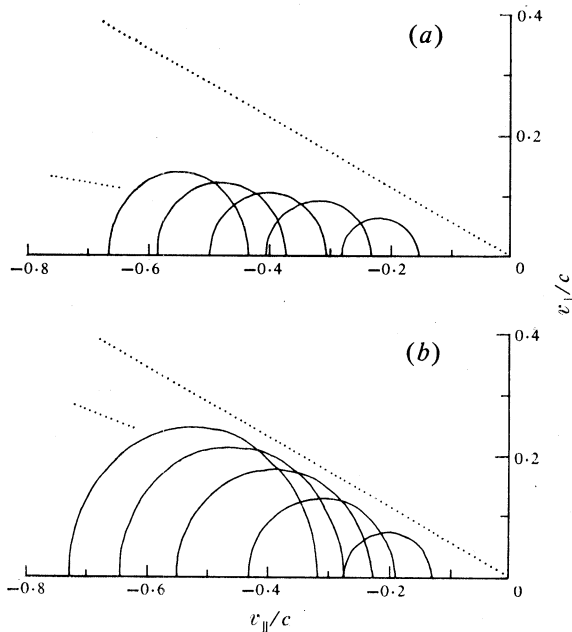


**Fig. 4.** Resonant ellipses for the curves in Fig. 1 for (a)  $N = 1$  and (b)  $N = 6$ . The sizes of the ellipses increase as  $\theta$  increases. In each case, the upper dotted line shows the loss-cone boundary and the lower dotted line an estimate of the half-width of the loss cone, as discussed in Section 6b.

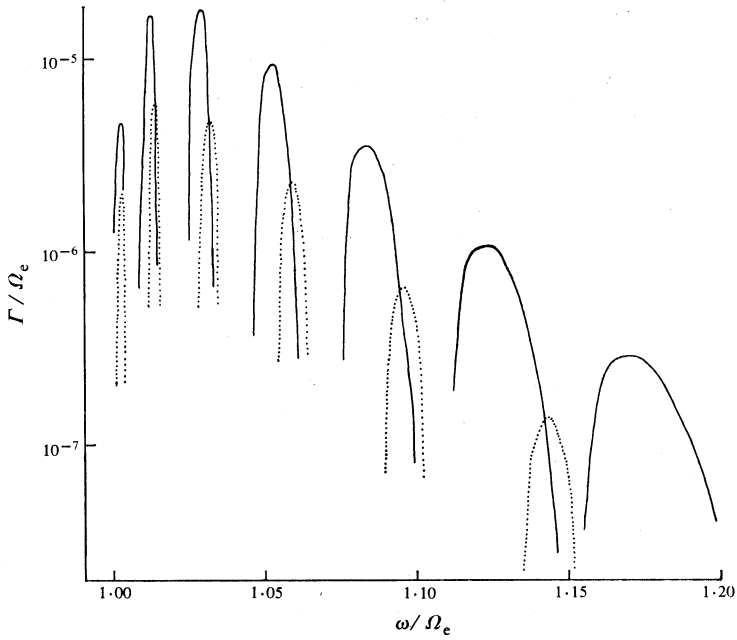


Fig. 5. As for Fig. 1 (p. 454) except for the o mode at  $s = 1$ . In this case  $\theta = 95^\circ, 100^\circ, 105^\circ, 110^\circ, 115^\circ, 120^\circ$  and  $125^\circ$  (from left to right).

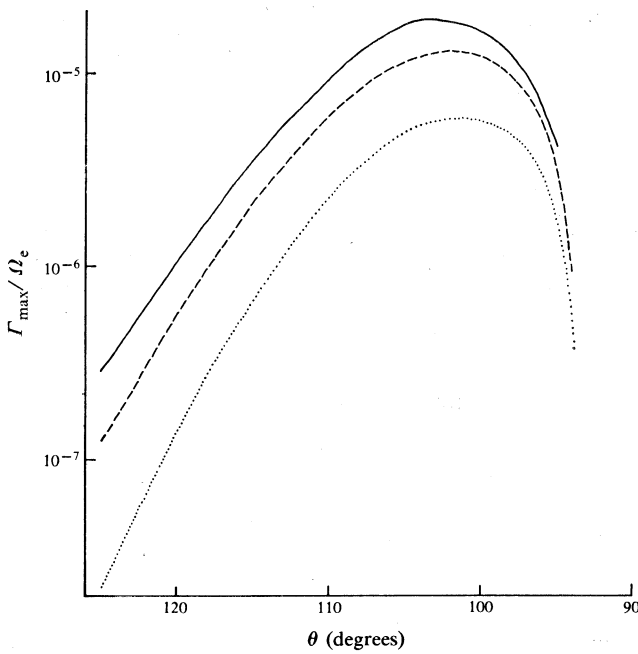


Fig. 6. As for Fig. 2 (p. 454) except for the o mode at  $s = 1$ .

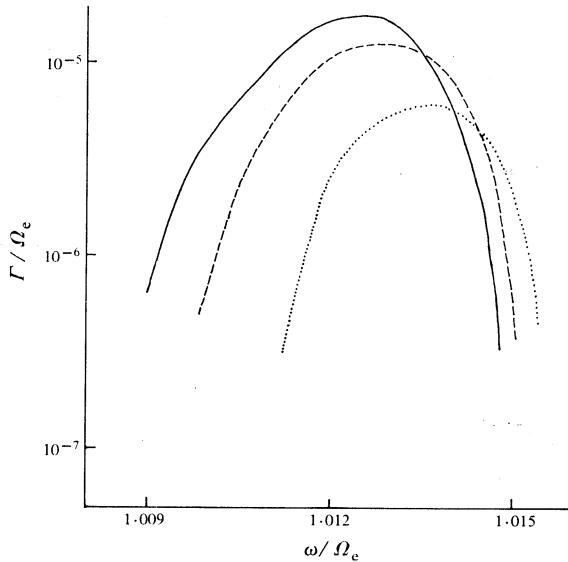


Fig. 7. As for Fig. 3 (p. 455) except for the o mode at  $s = 1$  and for  $\theta = 100^\circ$ . In this case we have  $\omega_{\max}/\Omega_e \approx 1.0136 - 0.0002N$  and  $\Delta\omega_{1/2}/\Omega_e \approx 0.0028$ .

The shape of the boundary curve for the x mode at  $s = 1$  (Fig. 11a) is qualitatively different from those for the o mode at  $s = 1$  (Fig. 11b) and the x mode at  $s = 2$  (Fig. 11c), due to the presence of a nose and a segment of the curve nearly parallel to the  $\theta$ -axis. Well above the nose, the curve may be approximated by the vacuum case  $\theta = \pi - \theta'$  with  $\theta'$  given by (14). Below the nose the shape of the curve is dominated by the dispersive properties of the x mode near its cutoff frequency. We return to this point in Section 5 below.

### (c) Half-maximum Growth Boundaries

Also plotted in Fig. 11 are the curves corresponding to the growth rates being equal to half their maximum values. The curves for increasing  $N$  are at an increasing distance from the curve  $V = 0$ , but to avoid confusion only the curves for  $N = 6$  are plotted. The half-maximum growth curves for  $N = 1, 3$  and  $6$  are plotted in Fig. 12 as a function of  $\delta\omega/\Omega_e$  and  $\theta$ , where  $\delta\omega$  (a negative quantity) is the frequency separation at fixed  $\theta$  between the half-maximum growth curves and the curve  $V = 0$ .

## 5. Suppression of Fundamental x Mode

For quite modest values of  $\omega_p/\Omega_e$ , growth of the x mode at  $s = 1$  can be strongly suppressed compared with that for negligible  $\omega_p/\Omega_e$ . This suppression may be understood semi-quantitatively in the following terms. In the limit of negligible  $\omega_p/\Omega_e$  there exists a favoured region of  $\omega$ - $\theta$  space where growth is most effective. As  $\omega_p/\Omega_e$  increases the curve  $V = 0$  moves in such a way as to decrease the region where resonance is possible. Suppression occurs when the favoured region for growth moves from inside to outside the curve  $V = 0$ .

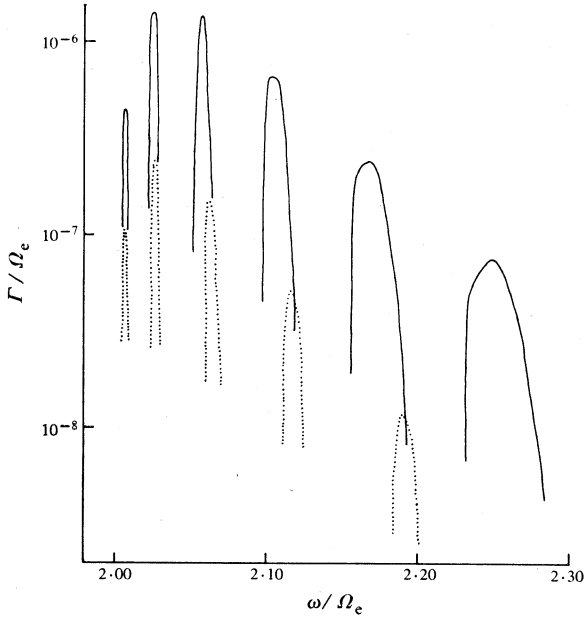


**Fig. 8.** As for Fig. 1 (p. 454) except for the x mode at  $s = 2$ . In this case  $\theta = 95^\circ, 100^\circ, 105^\circ, 110^\circ, 115^\circ$  and  $120^\circ$  (from left to right).

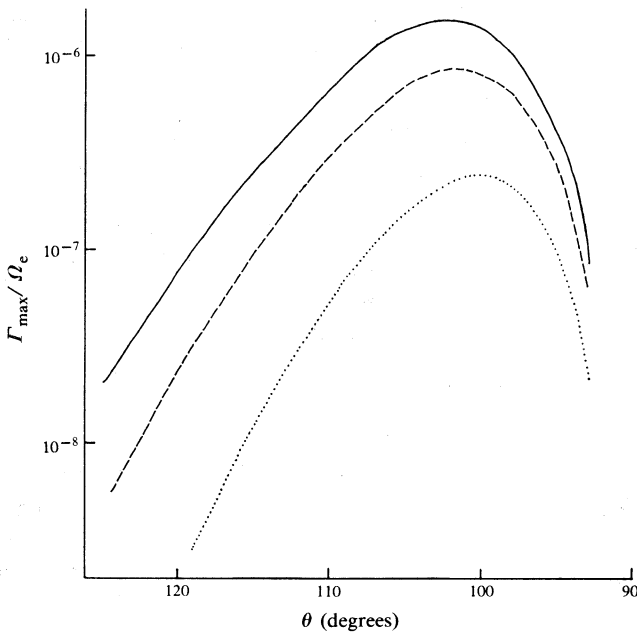


**Fig. 9.** As for Fig. 2 (p. 454) except for the x mode at  $s = 2$ .

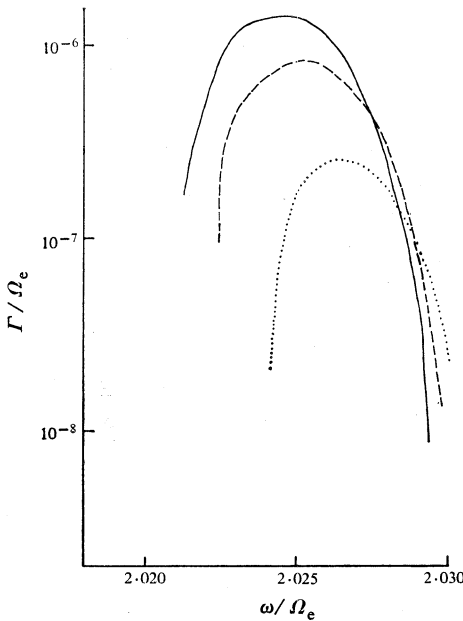


**Fig. 10.** As for Fig. 3 (p. 455) except for the x mode at  $s = 2$  and for  $\theta = 100^\circ$ . In this case we have  $\omega_{\max}/2\Omega_e \approx 1.0131 - 0.0001 N$  and  $\Delta\omega_{1/2}/2\Omega_e \approx 0.0023$ .

### (a) Numerical Results

The effect of increasing  $\omega_p/\Omega_e$  on the growth rates is illustrated in Fig. 13. For the x mode at  $s = 1$  (Fig. 13a), the maximum growth rate decreases rapidly with increasing  $\omega_p/\Omega_e \gtrsim 0.01$  and the position of the maximum moves to increasing  $|\theta - \frac{1}{2}\pi|$ . In contrast, the growth rate for the o mode at  $s = 1$  (Fig. 13b) is affected substantially only for  $\omega_p/\Omega_e \gtrsim 0.6$ , and for the x mode at  $s = 2$  (Fig. 13c) there is little noticeable effect for all  $\omega_p/\Omega_e \lesssim 1$ .

This suppression effect is also evident in the results of Lee *et al.* (1980) (cf. their Fig. 3). Note however that these authors plotted a function which differs from our growth rate by a factor of  $\omega_p^2$ .

### (b) Nose in Boundary Curve

The position of the nose in the boundary curve in Fig. 11a depends on the value of  $\omega_p/\Omega_e$ ; the variation of the boundary curve with  $\omega_p/\Omega_e$  is illustrated in Fig. 14. The position of this nose may be estimated as follows. The curve above the nose may be approximated by  $\theta = \pi - \theta'$  with  $\theta'$  given by (14). Below the nose, the x mode waves are close to their cutoff frequency  $\omega_x$  (cf. equation 7). Using the expression (8a) one finds, for  $\omega - \omega_x \lesssim \omega_p^2/\Omega_e$  and  $(\omega_p/\Omega_e)^2 \ll 1$ , that the dispersion relation may be approximated by expanding in powers of  $1 - X - Y \approx 2(\omega - \omega_x)/\Omega_e$ . To lowest order we find

$$k^2 c^2 = 2(\omega - \omega_x)\omega^2/(\omega - \Omega_e)(1 + \cos^2\theta). \quad (17)$$

Then  $\theta'$  is given by

$$\theta' \approx \arccos\left\{[(\omega - \Omega_e)/\{\omega(\omega - \omega_x)\}]^{\frac{1}{2}}\right\}. \quad (18)$$

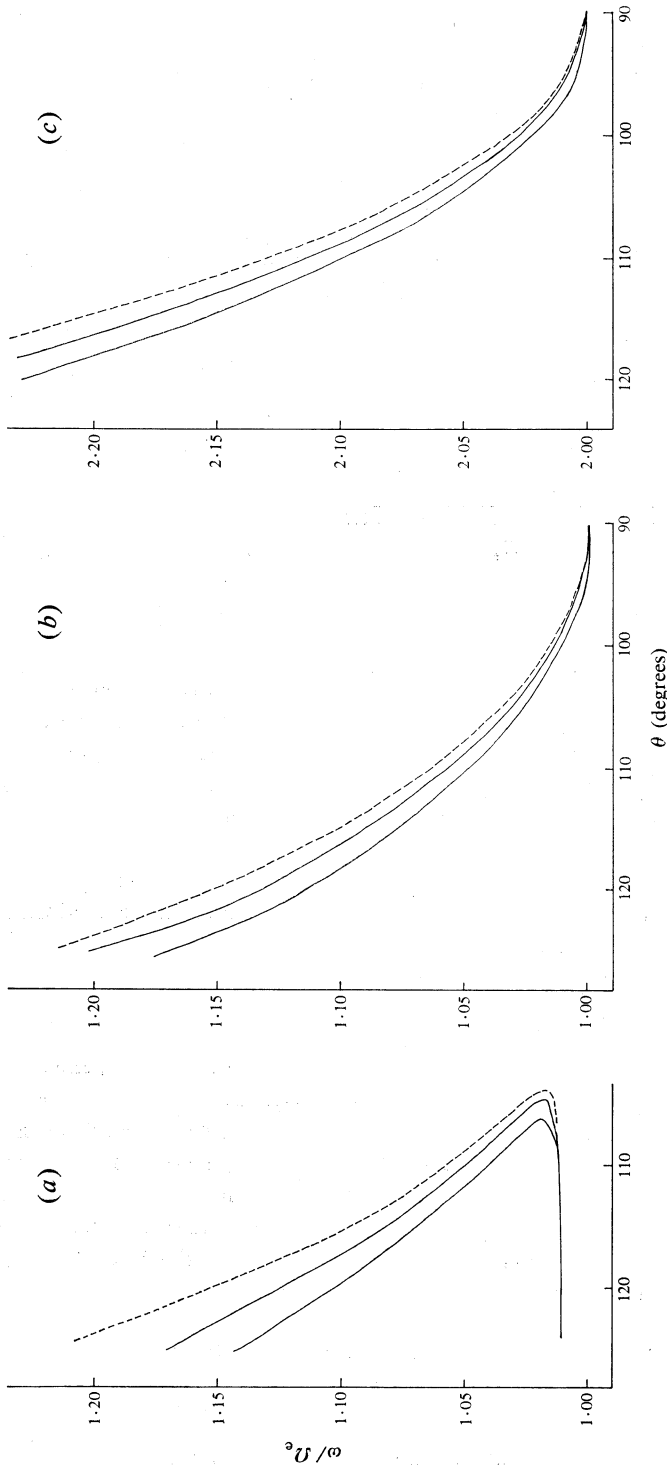
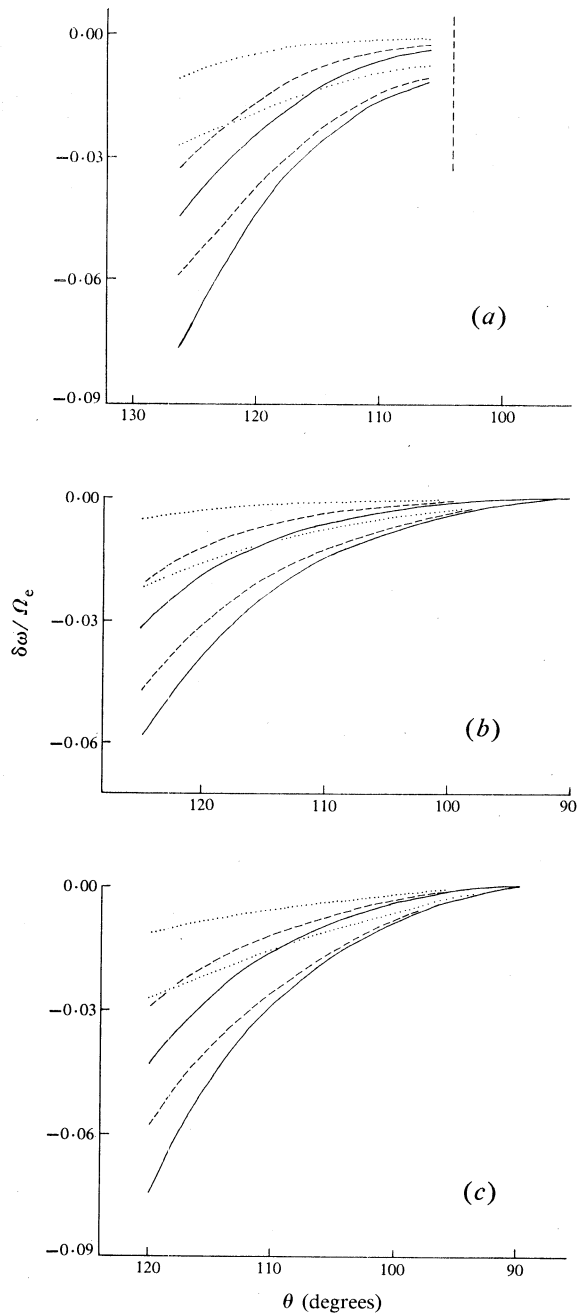


Fig. 11. Boundary (dashed) curves for  $\omega_p/\Omega_e = 0.1$  and for (a) the x mode at  $s = 1$  and (b) the o mode at  $s = 1$  and (c) the x mode at  $s = 2$ . Also plotted are the (solid) curves corresponding to the half-maximum growth points (at fixed  $\theta$ ) for  $N = 6$ .



**Fig. 12.** Half-maximum growth curves as a function of the frequency separation (for fixed  $\theta$  in Fig. 11) from the boundary curve for  $N = 1$  (dotted curves),  $N = 3$  (dashed curves) and  $N = 6$  (solid curves): (a) the x mode at  $s = 1$ , (b) the o mode at  $s = 1$  and (c) the x mode at  $s = 2$ . No emission occurs to the right of the dashed line at  $104^\circ$  in part a (cf. Fig. 2).

The position of the nose may be estimated from the intersection of the asymptotic curve, with  $\theta'$  given by (14), and the nearly horizontal curve for  $\omega \approx \omega_x$ , with  $\theta'$  given by (18). One finds that the nose should occur at

$$(\omega - \Omega_e)/\Omega_e \approx 2\omega_p^2/\Omega_e^2, \quad \theta' \approx \frac{1}{2}\pi - 2\omega_p/\Omega_e. \quad (19a, b)$$

The actual positions of the nose in Fig. 14 are reasonably well approximated by equations (19) for  $\omega_p^2/\Omega_e^2 \ll 1$ .

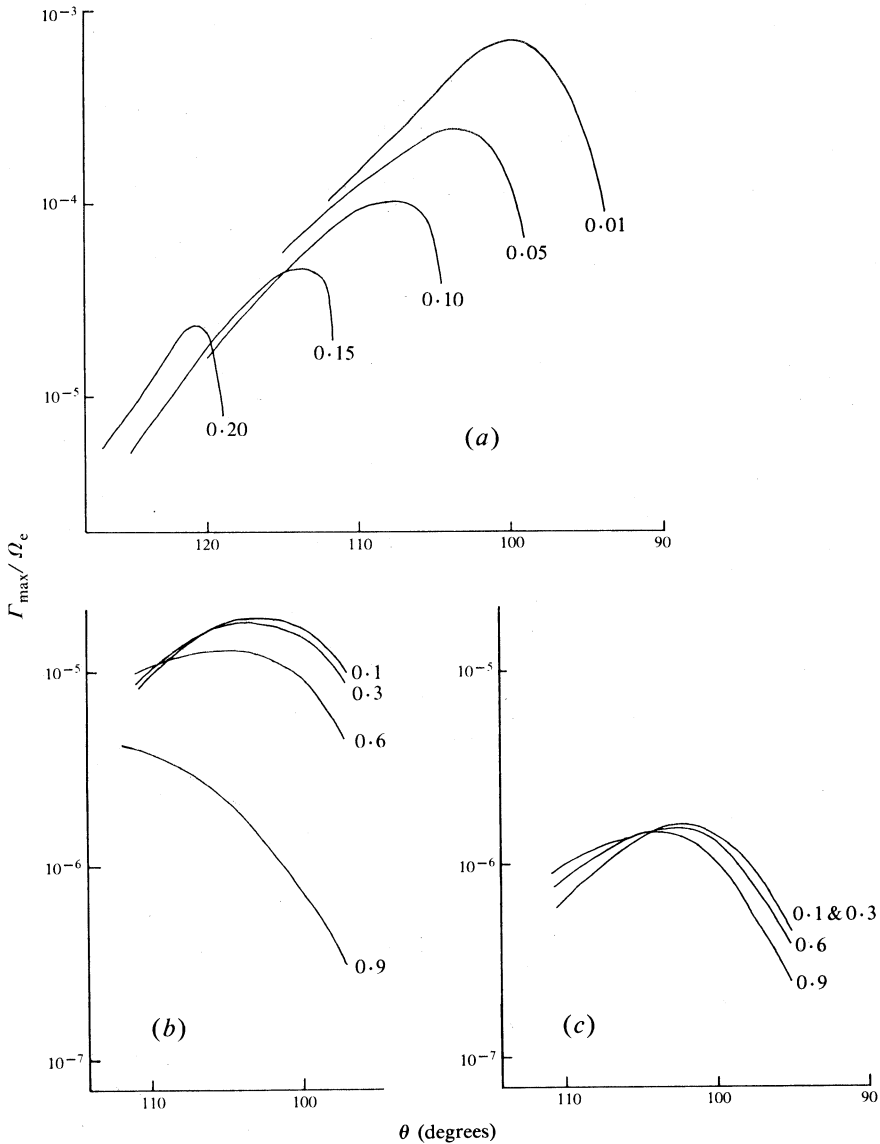


**Fig. 13.** Maxima (in  $\omega$ ) of the growth rates as a function of  $\theta$  for the ranges of values of  $\omega_p/\Omega_e$  indicated on the curves: (a) the x mode at  $s = 1$ , (b) the o mode at  $s = 1$  and (c) the x mode at  $s = 2$ . All curves are for  $N = 6$ .

(c) Interpretation

In practice there is a most favourable resonant ellipse, i.e. the one with the largest integrated value of  $\partial f/\partial p_{\perp}$  (weighted by a power of  $v_{\perp}$  which varies with  $s$ ). Let this ellipse be designated by its centre  $v_{\parallel} = v_m$  and its semi-major axis  $V = V_m$ . For ellipses with centres and/or semi-major axes substantially different from those optimum values, the growth rate is much less than the maximum value.

Suppose that  $\omega_p/\Omega_e$  is negligibly small. Then there always exist values of  $\omega$  and  $\theta$  which lie inside the boundary curve  $V = 0$  and which correspond to  $\cos \theta = v_m/c$  and  $V_m/c = \{\cos^2 \theta - 2(\omega - \Omega_e)/\Omega_e\}^{\frac{1}{2}}$  (cf. equations 5a and 6 with  $k = \omega/c$ ). Let this point in  $\omega$ - $\theta$  space be denoted by  $\theta = \theta_m$  and  $\omega = \omega_m$ .

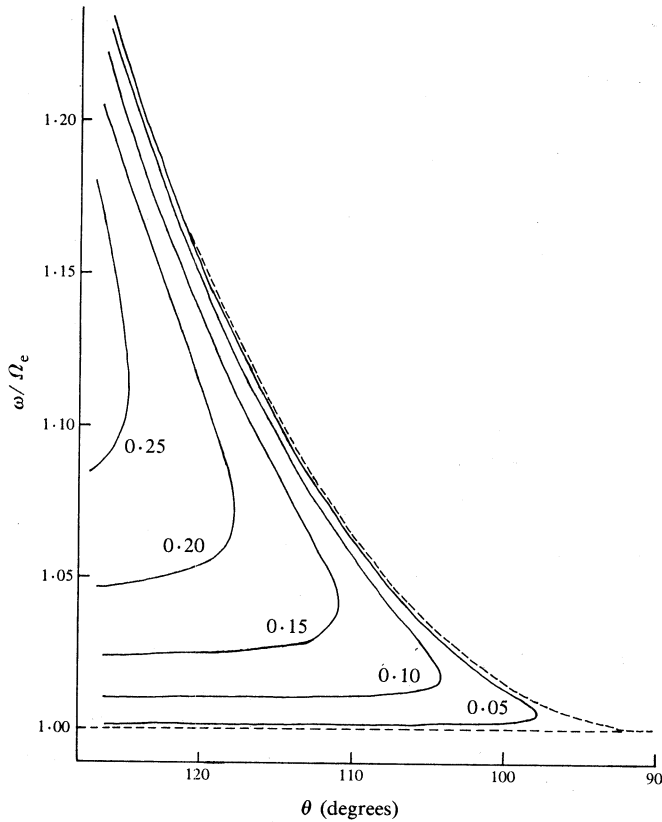


Fig. 14. Boundary curves for the x mode at  $s = 1$  for five values of  $\omega_p/\Omega_e$ . The dashed curve shows the limiting case  $\omega_p/\Omega_e = 0$ . We refer to the extremum point as a function of  $\theta$  as the nose.

As  $\omega_p/\Omega_e$  is increased the curve  $V = 0$  moves as shown in Fig. 14, and at some value  $(\omega_p/\Omega_e)_m$  it intersects the point  $\theta_m, \omega_m$ . For  $\omega_p/\Omega_e \gg (\omega_p/\Omega_e)_m$  the branch of the boundary curve above the nose corresponds to the centre of the ellipse being at  $|v_{\parallel}| \gg |v_m|$ . Consequently, resonant ellipses just to the left of this curve sample regions of velocity corresponding to  $|v_{\parallel}| \gg |v_m|$ . In practice the growth rate is then very small; for example, it falls off as  $\exp(-mv_{\parallel}^2/2KT)$  for a Maxwellian distribution.

For  $\omega_p/\Omega_e \gtrsim (\omega_p/\Omega_e)_m$  there is still a resonant ellipse corresponding to  $k_{\parallel} c/\omega = v_m/c$  and  $V_m/c = \{k_{\parallel}^2 c^2/\omega^2 - 2(\omega - \Omega_e)/\Omega_e\}^{1/2}$ ; it lies very close to the nearly horizontal branch of the curve in Fig. 14. The corresponding growth corresponds to the narrow peaks in Fig. 1, as discussed in Section 3a. The temporal growth rate is then small and is confined to an exceedingly small frequency range. The spatial growth rate remains quite large because of the small group speed in this case. Although we have not explored this particular regime in detail, several features are clear. First, to satisfy  $V_m^2/c^2 = v_m^2/c^2 - 2(\omega - \Omega_e)/\Omega_e$ , with  $V_m^2 \ll v_m^2$ , we require  $2(\omega - \Omega_e)/\Omega_e \approx v_m^2/c^2$ . However, for  $\omega \approx \omega_x$  and  $\omega_p^2 \ll \Omega_e^2$ , we have  $2(\omega - \Omega_e)/\Omega_e \approx 4\omega_p^2/\Omega_e^2$  and hence growth in this limiting case is favourable only for  $\omega_p/\Omega_e \approx |v_m|/2c$ ; from (29) in Section 6c below this is just the parameter regime where the suppression effect becomes important. Second, the growth is confined to an exceedingly narrow bandwidth. This places a strong limitation on any effective growth because  $\Omega_e$  must not change by more than the bandwidth of the growing waves across the source region (cf. Section 7 below).

In summary, the growth of the x mode at  $s = 1$  should be expressed for  $\omega_p/\Omega_e \gtrsim (\omega_p/\Omega_e)_m$ , with  $(\omega_p/\Omega_e)_m$  later to be identified as  $\approx |v_m|/2c$ . The suppression is stronger at small values of  $\cos\theta$ , as is apparent from the sharp cutoffs at small  $\cos\theta$  in the curves of Fig. 2. Growth near the cutoff, with  $k^2 c^2 \ll \omega^2$ , is possible and may be favourable for  $\omega_p/\Omega_e \approx |v_m|/2c$ , but we have not explored this point in detail.

## 6. Semi-quantitative Theory of Loss-cone Driven Cyclotron Masers

In this section we formulate a semi-quantitative theory for loss-cone driven electron-cyclotron masers. The basis of the theory is a model for the range of resonant ellipses for which growth is effective. Under ideal circumstances the maximum growth rate can approach the value (Melrose *et al.* 1982)

$$\frac{\Gamma_{\max}}{\Omega_e} \approx \pi \left( \frac{\omega_p}{\Omega_e} \right)^2 \frac{\delta n}{n_C} \frac{c^2}{V_m v_m}, \quad (20)$$

where  $v_m$  and  $V_m$  denote the centre and semi-major axis respectively of the most favourable ellipse, and  $\delta n$  is defined in terms of the value  $f = f_m$  of the distribution function at the edge of the loss cone at  $v_{\parallel} \approx v_m$  and  $v_{\perp} \approx V_m$ , with

$$\delta n = 2\pi m^3 V_m^2 |v_m| f_m. \quad (21)$$

In (20) the ratio  $\omega_p^2/n_C = e^2/\epsilon_0 m$  is independent of the number density of cold electrons.

The questions we address in formulating the semi-quantitative theory include estimates of (i) the bandwidth  $\Delta\omega$  and (ii) the angular width  $\Delta\theta$  of the growing waves, (iii) the dependence of the growth rate on  $\omega_p/\Omega_e$ , (iv) the coherence volume of the radiation and (v) the relative magnitude of o and x mode growth rates.

### (a) The Model

In Fig. 4 it is apparent that favourable ellipses lie entirely within the loss cone. Furthermore they do not touch the edge of the loss cone at  $\alpha = \alpha_0$  but remain inside the line  $\alpha = \alpha_0$  by an amount,  $\Delta\alpha$  say, dependent on the steepness of the gradient in  $f$ , i.e. dependent on  $N$  in our case. It is reasonable to assume that the favourable resonant ellipses correspond to ranges  $\Delta v_c$  and  $\Delta V$  of centres and semi-major axes about the optimum values  $v_m$  and  $V_m$  respectively.

Inspection of Fig. 4 shows that  $v_m$  and  $V_m$  are related by

$$V_m \approx |v_m| \sin \alpha_0 \approx |v_m| \alpha'_0, \tag{22}$$

where in the final approximate equality we assume  $\alpha'_0 = \pi - \alpha_0 \ll 1$ . For a fixed centre the range of  $V$  is determined by the range of  $\alpha$ :

$$\Delta V \approx |v_m| \Delta \alpha. \tag{23}$$

**Table 1. Maximum growth rate  $\Gamma_{\max}$  for x mode with  $s = 1$  and for  $N = 6$  in equations (12) compared with negative (damping) contribution  $\Gamma_0$  from cold electrons**

The hot (H) and cold (C) properties are related by  $n_c = 100 n_H$  and  $T_c = 0.1 T_H$ , and  $v_c = v_{\parallel}$  is the centre of the resonant circle. The rapid fall-off of  $|\Gamma_0|$  with increasing  $\theta$  may be attributed to the dependence of a Maxwellian distribution proportional to  $\exp(-mv_c^2/2KT)$

$\theta$ (deg)	$ v_c /c$	$\Gamma_{\max}/\Omega_e$	$\Gamma_0/\Omega_e$	$(\Gamma_{\max} + \Gamma_0)/\Omega_e$
105	0.201	$6.5 \times 10^{-5}$	$-2.30 \times 10^{-4}$	$-1.65 \times 10^{-4}$
106	0.233	$9.7 \times 10^{-5}$	$-1.18 \times 10^{-4}$	$-2.11 \times 10^{-5}$
107	0.256	$1.01 \times 10^{-4}$	$-5.2 \times 10^{-5}$	$4.9 \times 10^{-5}$
108	0.277	$1.03 \times 10^{-4}$	$-1.07 \times 10^{-5}$	$9.2 \times 10^{-5}$
109	0.296	$1.01 \times 10^{-4}$	$-4.3 \times 10^{-6}$	$9.6 \times 10^{-5}$
110	0.313	$9.0 \times 10^{-5}$	$-1.86 \times 10^{-6}$	$8.8 \times 10^{-5}$
115	0.392	$4.4 \times 10^{-5}$	$-1.85 \times 10^{-8}$	$4.4 \times 10^{-5}$
120	0.464	$1.54 \times 10^{-5}$	$-1.82 \times 10^{-11}$	$1.54 \times 10^{-5}$
125	0.528	$4.5 \times 10^{-6}$	$-7.8 \times 10^{-15}$	$4.5 \times 10^{-6}$

The range of centres is more strongly model dependent. From Fig. 4 we would estimate

$$\Delta v_c \approx |v_m|. \tag{24a}$$

However, there is a constraint which in its severest form would require  $\Delta v_c$  much less than  $|v_m|$ . This is the effect of thermal particles. In  $v_{\perp}$ - $v_{\parallel}$  space the thermal particles are concentrated in a central circle. For any resonant ellipse which intersects this central circle there is a large damping contribution from the thermal electrons. This is shown for a particular case in Table 1. It is reasonable to conclude that growth occurs only for those ellipses which lie outside this central circle. The severest form of constraint is to assume that the inner edge of the resonant ellipses at  $|v_{\parallel}| = |v_c| - V$  is constrained to touch this central circle. Then we have

$$\Delta v_c \approx \Delta V. \tag{24b}$$

In practice  $\Delta v_c$  is likely to be between these two limits. Probably

$$\Delta v_c \approx V_m \tag{24c}$$

is a plausible value. (Our numerical calculations do not allow us to discuss this point quantitatively because of the neglect of the damping by the cold electrons, except in the illustrative example in Table 1.)

Equations (22)–(24) constitute our semi-quantitative model for the location of the favourable ellipses. We now use (5a) and (6) to relate these parameters to those of the emitted radiation.

(b) *Estimates of  $\theta_m$ ,  $\omega_m$ ,  $\Delta\theta$  and  $\Delta\omega$* 

Let us assume that  $k$  is close to  $\omega/c$ . In practice this excludes only emission very close to  $\omega_x$  for the x mode at  $s = 1$ . Then (5a) implies

$$\cos\theta_m = v_m/c, \quad (25)$$

and (6) implies

$$(\omega_m - s\Omega_e)/s\Omega_e = \frac{1}{2}(\cos^2\theta_m - V_m^2/c^2). \quad (26)$$

From Figs 3, 7 and 10 our numerical results imply  $\theta_m \approx 110^\circ$  and  $(\omega_m - \Omega_e)/\Omega_e \approx 0.05$  for the x mode at  $s = 1$ , and  $\theta_m \approx 100^\circ$  and  $(\omega_m - s\Omega_e)/s\Omega_e \approx 0.013$  for the o mode at  $s = 1$  and the x mode at  $s = 2$ . The x mode at  $s = 1$  is an exception because of the suppression effect, which is not negligible for  $\omega_p/\Omega_e = 0.1$ . From Fig. 13a one concludes that for sufficiently small  $\omega_p/\Omega_e$ ,  $\theta_m$  would also occur at  $\approx 100^\circ$  for the x mode at  $s = 1$ . Now  $\theta_m = 100^\circ$  implies  $|v_m|/c = 0.17$ , which is close to the value expected from the thermal speed of electrons at  $10^8$  K,  $(KT/m)^{\frac{1}{2}} = 0.13c$ . The estimate of  $(\omega_m - s\Omega_e)/s\Omega_e$  then implied by (26) and (22), with  $\sin\alpha_0 = \frac{1}{2}$ , is 0.011, which is in satisfactory agreement with our numerical results for the o mode at  $s = 1$  and the x mode at  $s = 2$ . For the x mode at  $s = 1$  equation (26) is valid only for  $\omega_m - \omega_x \gg \omega_x - \Omega_e$ , which is not the case for  $\omega_p/\Omega_e = 0.1$ . It may be concluded that (25) and (26) are satisfactory except for the x mode at  $s = 1$ , where they apply only for sufficiently small  $\omega_p/\Omega_e$ .

The range  $\Delta\theta$  follows from

$$\Delta\theta \approx \Delta v_e/c, \quad (27)$$

where we assume  $\sin\theta_m \approx 1$ . From our numerical calculations for the o mode at  $s = 1$  and for the x mode at  $s = 2$  we estimate  $\Delta\theta \approx 10^\circ$ ; for example, from the half-maximum growth points in Figs 6 and 9. These results are consistent with  $\Delta v_e$  being given by (24a). However, the constraint imposed by the cold electrons was not included in our numerical calculations, and this result in no way invalidates the arguments leading to the smaller estimates (24b) and (24c) of  $\Delta\theta$ .

Finally, the range of frequencies at fixed  $\theta$  follows from (26) and (23):

$$\frac{\Delta\omega}{s\Omega_e} \approx \frac{V_m}{c} \frac{|v_m|}{c} \Delta\alpha. \quad (28)$$

Before inserting numerical values we need to estimate  $\Delta\alpha$ . For a fit indicated in Fig. 4 we find the empirical estimate  $\Delta\alpha \approx 2\alpha'_0/3N^{\frac{1}{2}}$ . For the x mode at  $s = 1$  we have  $v_m/c \approx -0.3$ , and then (28) with  $V_m = \frac{1}{2}|v_m|$  and  $\alpha'_0 = \frac{1}{2}\pi$  gives  $\Delta\omega/\Omega_e \approx 0.02/N^{\frac{1}{2}}$ . The width at half-maximum growth for  $\theta = 110^\circ$  and  $N = 6$  corresponds to  $\Delta\omega/\Omega_e \approx 0.01$ . For the o mode at  $s = 1$  and the x mode at  $s = 2$ ,  $v_m/c \approx -0.17$  is a better fit. Then (28) gives  $\Delta\omega/s\Omega_e \approx 0.005/N^{\frac{1}{2}}$ . For  $\theta = 100^\circ$  and  $N = 6$  our numerical results give  $\Delta\omega/s\Omega_e = 0.003$  and  $0.002$  in these two cases respectively. It may be concluded that (28) gives a reasonable estimate of the width at half-maximum growth.

(c) *Suppression of x Mode at  $s = 1$* 

Our semi-quantitative model may be used to estimate the value  $(\omega_p/\Omega_e)_m$  at which suppression of the x mode at  $s = 1$  becomes an important effect. From the argument

given in Section 5c the suppression must be a substantial effect for all values of  $\omega_p/\Omega_e$  for which the point  $\omega_m, \theta_m$  lies outside the boundary curve in  $\omega-\theta$  space, where  $\omega_m, \theta_m$  are the values for maximum growth in the limit of arbitrarily small  $\omega_p/\Omega_e$ . Comparison of equations (19) with (25) and (26) shows that the nose crosses the point  $\omega_m, \theta_m$  for  $\omega_p/\Omega_e \approx \frac{1}{2}|v_m|/c$ . Therefore we estimate

$$(\omega_p/\Omega_e)_m \approx \frac{1}{2}|v_m|/c. \tag{29}$$

In our case we have  $|v_m|/c \approx 0.17$  for small  $\omega_p/\Omega_e$ , and then (29) implies that suppression is a substantial effect for  $\omega_p/\Omega_e \gtrsim 0.08$ . It is clear from Fig. 13a that the maximum growth rate for  $\omega_p/\Omega_e \approx 0.08$  is down by at least a factor of five from the unsuppressed value. Some suppression is evident even for  $\omega_p/\Omega_e \approx 0.05$ .

The sharp cutoff in the curves at  $\theta = 104^\circ$  in Fig. 2 is due to this suppression effect. On the basis of (25) and (29) we would predict a cutoff at  $|\cos \theta| \approx 2(\omega_p/\Omega_e)$ , i.e. at  $|\cos \theta| = 0.2$  for  $\omega_p/\Omega_e = 0.1$ . The predicted angle is  $\theta = 102^\circ$ , in satisfactory agreement with the value  $104^\circ$  evident from Fig. 2.

(d) *Coherence Volume*

An important observational feature of maser emission is its high brightness temperature. The brightness temperature  $T_b$  is related to the energy density  $W$  in the radiation by

$$KT_b = WV_{\text{coh}}, \tag{30}$$

where

$$V_{\text{coh}} \approx \left\{ \left( \frac{\omega}{2\pi c} \right)^3 \frac{\Delta\omega}{\omega} 2\pi \Delta\theta \sin \theta \right\}^{-1} \tag{31}$$

is the coherence volume of the radiation. Now  $W$  is restricted to  $\lesssim \frac{1}{2} \delta n m V_m^2$ , and is likely to be very much less than this value (Melrose and Dulk 1982a, 1982b). A high brightness temperature requires a large coherence volume, and the coherence volume is indeed large for a loss-cone driven cyclotron maser. Using (24a), (27) and (28) we find

$$V_{\text{coh}} \approx \left\{ 2\pi \left( \frac{\omega}{2\pi c} \frac{|v_m|}{c} \alpha'_0 \right)^3 \left( \frac{\Delta\alpha}{\alpha'_0} \right)^2 \right\}^{-1}. \tag{32}$$

For thermal radiation  $V_{\text{coh}}$  is of the order of a wavelength cubed, and (32) implies that for the maser emission  $V_{\text{coh}}$  exceeds the thermal value by a factor of order  $(c/|v_m| \alpha'_0)^3 (\alpha'_0/\Delta\alpha)^2$ .

(e) *Comparison of o and x Modes*

In our numerical calculations we found the growth rate for the o mode at  $s = 1$  to be smaller than that of the x mode at  $s = 1$  by a factor of about ten. Let us use our semi-quantitative model to estimate how the relative magnitudes of the growth rates for the o and x modes should depend on the parameters  $|v_m|/c$  and  $\alpha'_0$ . We assume that  $\omega_p/\Omega_e$  is sufficiently small that the growth of the x mode is not suppressed. Then the relative magnitudes of the growth rates can depend only on the polarizations of the two modes.

For  $\omega \approx \Omega_e \gg \omega_p$ , equation (8c) implies

$$T_x \approx \cos \theta, \quad T_o \approx -1/\cos \theta. \quad (33a, b)$$

In (10) the dependence on the mode for  $n_\sigma \approx 1$  and negligible  $K_\sigma$  (which is the case here) is only on  $T_\sigma$ , and we have

$$A_1^{(\sigma)}(\mathbf{p}, \mathbf{k}) \approx \frac{\pi^2 e^2 v_\perp^2}{\omega(1+T_\sigma^2)} |(\cos \theta - v_{\parallel}/c)T_\sigma + 1|^2. \quad (34)$$

For  $|\cos \theta| \ll 1$ , to a first approximation we may set  $T_x = 0$  and  $T_o = \infty$ , implying that inside the modulus squared the unit term dominates for the x mode and the other term for the o mode. Now on integrating around the resonant ellipse,  $\cos \theta - v_{\parallel}/c$  ( $\approx (v_m - v_{\parallel})/c$ ) passes through zero, and the net contribution from the integral of  $(\cos \theta - v_{\parallel}/c)^2$  should be of order  $\cos^2 \theta$  smaller than the integral of unity. Thus, with  $\cos \theta \approx v_m/c$ , we expect

$$\Gamma_1^{(o)}/\Gamma_1^{(x)} \approx (v_m/c)^2. \quad (35)$$

In particular the ratio depends on the energy of the electrons driving the instability, but not on the loss-cone angle  $\alpha_0$ .

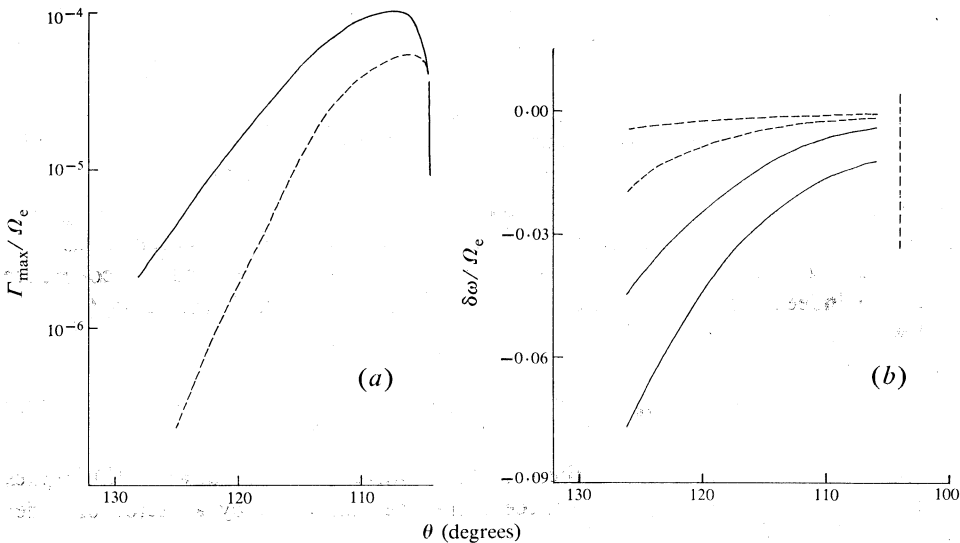


**Fig. 15.** Effect of changing the value of  $\alpha_0$  from  $150^\circ$  (solid curves) to  $170^\circ$  (dashed curves) on (a) the maximum growth for the x mode at  $s = 1$  and (b) the half-maximum growth points. In part a the curve for  $\alpha_0 = 150^\circ$  is the same as the  $N = 6$  (solid) curve in Fig. 2 and in part b the curves for  $\alpha_0 = 150^\circ$  are the same as the  $N = 6$  (solid) curves in Fig. 12a.

In our numerical calculations  $v_m/c$  is roughly  $-0.3$  (cf. Fig. 4), and  $\Gamma_1^{(o)}/\Gamma_1^{(x)}$  is of order  $0.1$ . These results are consistent with (35). Note however that the value  $v_m/c \approx -0.3$  is affected by the suppression effect and we have neglected the suppression in deriving (35). Alternatively, in the absence of suppression  $v_m/c$  is of order  $-0.17$ , implying  $(v_m/c)^2 \approx 0.03$ . The suppression affects the x mode, but not the

o mode, effectively increasing the ratio by a factor of order ten for  $\omega_p/\Omega_e \approx 0.1$ . It may be concluded that even when the suppression is significant, it is reasonable to use (35) with  $v_m/c$  identified as the value for maximum growth of the x mode at  $s = 1$ .

(f) *Dependence on  $\alpha'_0$*

Finally, let us return to the quantitative estimate (20). The maximum value of  $\Gamma_{\max}/\Omega_e$  according to Fig. 14 is probably of order  $10^{-3}$  for sufficiently small  $\omega_p/\Omega_e$ . Assuming  $\Omega_e/2\pi = 3$  GHz,  $\alpha'_0 = 30^\circ$  and  $n_H = 10^{13} \text{ m}^{-3}$ , as in our numerical calculations, with  $v_m/c \approx -0.3$  and  $V_m \approx \frac{1}{2}|v_m|$ , equation (20) gives  $\Gamma_{\max}/\Omega_e \approx 10^{-3}$  as required.

One other feature of (20) which we might test is the dependence on  $\alpha'_0$ . With  $V_m/|v_m| \approx \sin \alpha'_0$  from (22), the  $V_m$  dependences in (20) and (21) imply that  $\Gamma_{\max}$  is proportional to  $\sin \alpha'_0$ . Unfortunately, the details of our numerical code precluded treatment of the case of very small  $\sin \alpha'_0$ . In Fig. 15 we compare the cases  $\alpha'_0 = 150^\circ$  and  $170^\circ$ . The difference in the magnitude of the growth rates is a factor of two. This compares reasonably with the ratio  $\sin 150^\circ/\sin 170^\circ = 2.9$ .

## 7. Application to DAM

As an illustration of the use of the results derived here let us discuss the application to Jovian emission DAM. In our earlier discussion of this application (Hewitt *et al.* 1981) we did not have an adequate understanding of the semi-quantitative dependence of  $\Delta\theta$  and  $\Delta\omega$  on the parameters  $v_m$ ,  $\alpha_0$  and  $\Delta\alpha$ , and of the dependence of the growth rate on these parameters and on  $\omega_p/\Omega_e$ . Hence we concentrate on these features.

From the work of Dulk (1967), it appears that DAM is emitted on the surface of a hollow cone with  $\theta_m \approx 80^\circ$  and  $\Delta\theta \approx 1^\circ$ . Using (25) and (27), the implied energy of the emitting electrons is  $\frac{1}{2}mv_m^2 \approx 8$  keV and with  $\Delta v_c = |v_m|\Delta\alpha$  the implied value of  $\Delta\alpha$  is  $\approx 6^\circ$ . Then using (28) and  $\Delta\alpha \approx 2\alpha'_0/3N^{\frac{1}{2}}$ , the expected relative bandwidth of the radiation is  $\Delta\omega/\Omega_e \approx 5 \times 10^{-4} N^{\frac{1}{2}}$ . Assuming  $N \approx 4$ , one would expect a bandwidth of  $\approx 20$  kHz for emission at  $\approx 20$  MHz. Such narrow frequency structures have been observed in DAM by Ellis (1974, 1979).

Using these estimates, the coherence volume (32) is  $V_{\text{coh}} \approx 3 \times 10^7 \text{ m}^3$  at  $\omega/2\pi \approx 20$  MHz. Dulk *et al.* (1967) and Dulk (1970) have estimated the brightness temperature of DAM to be  $\gtrsim 10^{17}$  K. However, the large coherence volume implies that such a high brightness temperature corresponds to a relatively modest radiative energy density in the source. Specifically we have  $KT_b/V_{\text{coh}} \approx 5 \times 10^{-14} \text{ J m}^{-3}$  for  $T_b \approx 10^{17}$  K, and this energy density is much less than that of 8 keV electrons according to our estimates below.

The most severe constraint on the maser mechanism arises from the narrow bandwidth. The path length for amplification is limited by the fact that  $\Omega_e$  must not change by more than  $\Delta\omega$  along it. Assuming  $|\text{grad } \Omega_e| \approx \Omega_e/R_J$ , where  $R_J$  is the radius of Jupiter, the effective amplification length is

$$L_A \approx (\Delta\omega/\Omega_e)R_J. \quad (36)$$

Assuming that more than ten e-folding growths are required, growth is effective only for

$$\Gamma_{\max} \gtrsim 10c/L_A. \quad (37)$$

Now using (20), (22), (28), (36) and (37) and estimating  $\delta n$  by  $\alpha_0^2 n_H$ , where  $n_H$  is the number density of  $\gtrsim 8$  keV electrons, we find

$$n_H \gtrsim \frac{10 n_C}{\pi \omega_p^2 R_J} \frac{\Omega_e c}{\alpha_0^2 \Delta \alpha}. \quad (38)$$

Inserting numerical values, with  $\Omega_e/2\pi \approx 20$  MHz, the inequality (38) requires  $n_H \gtrsim 5 \times 10^7 \text{ m}^{-3}$ .

A maser theory such as that developed here applies only when the growth rate is less than the bandwidth of the growing waves. For the values estimated above the condition  $\Gamma_{\text{max}} \lesssim \Delta\omega$  implies  $n_H \lesssim 10^8 \text{ m}^{-3}$ , so use of the maser theory is only marginally justified. (However, if our estimate of  $\Delta\theta$  were increased from  $1^\circ$  to  $2^\circ$ , the right-hand sides of the inequalities  $n_H \gtrsim 5 \times 10^7 \text{ m}^{-3}$  and  $n_H \lesssim 10^8 \text{ m}^{-3}$  would be altered by multiplication factors of  $2^{-3}$  and 2 respectively.) Both this inequality and (38) apply only for  $\omega_p/\Omega_e \ll \frac{1}{2} |v_m|/c$ , i.e. for  $n_C \ll 3 \times 10^{10} \text{ m}^{-3}$ .

Further discussion of the application to DAM requires a physical model for the formation and evolution of the distribution of radiating electrons in the source region. No such satisfactory model is available.

## 8. Concluding Remarks

In the Introduction we emphasized that the instability under discussion is of class SM and that the significance of this class of instabilities has been recognized only recently. In these concluding remarks we comment on the loss-cone driver of the instability.

Any maser requires a pump, and the pump must operate on a time scale comparable with or shorter than the radiative decay time of the state being pumped. In our classical maser, the occupation number in discrete states is replaced by a continuous distribution function  $f(p_\perp, p_\parallel)$ , and an inverted population requires  $\partial f/\partial p_\perp > 0$ . The pump must either supply electrons with large  $p_\perp$  or remove electrons with small  $p_\perp$ . The only obvious candidate involves a loss cone which allows electrons with small  $p_\perp/p_\parallel$  to escape from a magnetic trap. The pump then involves a source of energetic electrons within the trap. The maser emission itself causes enhanced scattering into the loss cone (Wu *et al.* 1981; Melrose *et al.* 1982; Melrose and Dulk 1982*a*) and the pump must operate on a time scale shorter than that in which the electrons would be lost through this enhanced scattering into the loss cone.

The only well-formulated idea for a pump is that proposed by Wu and Lee (1979) and which evidently operates in the source region for TKR. Electrons directed downward towards the Earth reflect if they are outside the loss cone and precipitate if they are inside the loss cone. The reflected electrons then include none inside an upward directed loss cone. However, even in this case, it is not obvious how the pump modulates the emission of TKR. It is clear from observations of TKR, and the more so for DAM, that the emission is far from uniform and constant across the source region. Bursts of radiation seem to require some additional mechanism which modulates the downward flow of electrons on a relatively short time scale. A parallel electric field, for example in the form of an electrostatic shock or double layer, is a likely candidate.

It may be concluded that although the pump for a loss-cone driven maser has been identified in general terms, further work on this important aspect of the maser mechan-

ism is required. In particular, the processes which tend to form a loss-cone distribution on a longer time scale must be modulated on a time scale of a few tens of growth times in order for the maser to operate effectively.

## References

- Bekefi, G. (1966). 'Radiation Processes in Plasmas' (Wiley: New York).
- Bekefi, G., Hirshfield, J. L., and Brown, S. D. (1961). *Phys. Rev.* **122**, 1037.
- Benson, R. F., and Calvert, W. (1979). *Geophys. Res. Lett.* **7**, 959.
- Briggs, R. J. (1964). 'Electron-stream Interaction with Plasmas' (M.I.T. Press: Cambridge, Mass.).
- Chang, D. B. (1963). *Astrophys. J.* **138**, 1231.
- Chu, R. K., and Hirshfield, J. L. (1978). *Phys. Fluids* **21**, 461.
- Dulk, G. A. (1967). *Icarus* **7**, 173.
- Dulk, G. A. (1970). *Astrophys. J.* **159**, 671.
- Dulk, G. A., Rayhner, B., and Lawrence, R. (1967). *Astrophys. J.* **150**, L117.
- Ellis, G. R. A. (1965). *Radio Sci. D* **69**, 1513.
- Ellis, G. R. A. (1974). *Proc. Astron. Soc. Aust.* **2**, 236.
- Ellis, G. R. A. (1979). An atlas of selected spectra of the Jupiter S-bursts. Physics Department, Univ. of Tasmania.
- Ellis, G. R. A., and McCulloch, P. M. (1963). *Aust. J. Phys.* **16**, 380.
- Fung, P. C. W. (1966). *Plan. Space Sci.* **14**, 469.
- Gaponov, A. V. (1959a). *Izv. UVZ Radiofizika* **2**, 450.
- Gaponov, A. V. (1959b). *Izv. UVZ Radiofizika* **2**, 836.
- Goldreich, P., and Lynden-Bell, D. (1969). *Astrophys. J.* **156**, 59.
- Goldstein, M. L., and Eviatar, A. (1972). *Astrophys. J.* **175**, 275.
- Goldstein, M. L., and Eviatar, A. (1979). *Astrophys. J.* **230**, 261.
- Goldstein, M. L., and Goertz, C. K. (1982). 'Theories of Radio Emission and Plasma Waves', In 'Physics of the Jovian Magnetosphere' (Ed. A. J. Dessler) (Cambridge Univ. Press).
- Goldstein, M. L., and Thieman, J. R. (1981). *J. Geophys. Res.* **86**, 8569.
- Hewitt, R. G., Melrose, D. B., and Rönmark, K. G. (1981). *Proc. Astron. Soc. Aust.* **4**, 226.
- Hirshfield, J. L., and Bekefi, G. (1963). *Nature* **198**, 20.
- Holman, G. D., Eichler, D., and Kundu, M. (1980). In 'Radio Physics of the Sun' (Eds M. Kundu and T. Gergeley), p. 457 (D. Reidel: Dordrecht).
- Lee, L. C., Kan, J. R., and Wu, C. S. (1980). *Plan. Space Sci.* **28**, 703.
- Lee, L. C., and Wu, C. S. (1980). *Phys. Fluids* **23**, 1348.
- Melrose, D. B. (1973). *Aust. J. Phys.* **26**, 229.
- Melrose, D. B. (1976). *Astrophys. J.* **207**, 651.
- Melrose, D. B. (1980a). 'Plasma Astrophysics', Vol. I (Gordon and Breach: New York).
- Melrose, D. B. (1980b). 'Plasma Astrophysics', Vol. II (Gordon and Breach: New York).
- Melrose, D. B., and Dulk, G. A. (1982a). *Astrophys. J.* **259**, 844.
- Melrose, D. B., and Dulk, G. A. (1982b). *Astrophys. J.* **259**, L41.
- Melrose, D. B., Rönmark, K. G., and Hewitt, R. G. (1982). *J. Geophys. Res.* **87**, 5140.
- Omidi, N., and Gurnett, D. A. (1982). *J. Geophys. Res.* **87**, 2377.
- Sagdeev, R. Z., and Shafranov, V. C. (1960). *Sov. Phys. JETP* **12**, 130.
- Schneider, J. (1959). *Phys. Rev. Lett.* **2**, 504.
- Sprangle, P., and Drobot, A. T. (1977). *IEEE Trans. Microwave Theory Tech.* **25**, 528.
- Stix, T. H. (1962). 'The Theory of Plasma Waves' (McGraw-Hill: New York).
- Twiss, R. Q. (1958). *Aust. J. Phys.* **11**, 564.
- Winglee, R. (1982). Interrelation between azimuthal bunching and semirelativistic maser cyclotron instabilities. *Plasma Phys.* (in press).
- Wu, C. S., and Lee, L. C. (1979). *Astrophys. J.* **230**, 621.
- Wu, C. S., Tsai, S. T., Xu, M. J., and Shen, J. W. (1981). *Astrophys. J.* **248**, 384.
- Wu, C. S., Wong, H. K., Gorney, D. J., and Lee, L. C. (1982). *J. Geophys. Res.* **87**, 4476.

